nature COMMUNICATIONS

ARTICLE

Received 20 Apr 2012 | Accepted 30 Jul 2012 | Published 4 Sep 2012

DOI: 10.1038/ncomms2029

Ultrafast magnetization enhancement in metallic multilayers driven by superdiffusive spin current

Dennis Rudolf[1,*], Chan La-O-Vorakiat[2,*], Marco Battiato[3,*], Roman Adam[1], Justin M. Shaw[4], Emrah Turgut[2], Pablo Maldonado[3], Stefan Mathias[2,5], Patrik Grychtol[1,2], Hans T. Nembach[4], Thomas J. Silva[4], Martin Aeschlimann[5], Henry C. Kapteyn[2], Margaret M. Murnane[2], Claus M. Schneider[1] & Peter M. Oppeneer[3]

Uncovering the physical mechanisms that govern ultrafast charge and spin dynamics is crucial for understanding correlated matter as well as the fundamental limits of ultrafast spin-based electronics. Spin dynamics in magnetic materials can be driven by ultrashort light pulses, resulting in a transient drop in magnetization within a few hundred femtoseconds. However, a full understanding of femtosecond spin dynamics remains elusive. Here we spatially separate the spin dynamics using Ni/Ru/Fe magnetic trilayers, where the Ni and Fe layers can be ferro- or antiferromagnetically coupled. By exciting the layers with a laser pulse and probing the magnetization response simultaneously but separately in Ni and Fe, we surprisingly find that optically induced demagnetization of the Ni layer transiently enhances the magnetization of the Fe layer when the two layer magnetizations are initially aligned parallel. Our observations are explained by a laser-generated superdiffusive spin current between the layers.

[1] Peter Grünberg Institut PGI-6 & JARA-FIT, Research Centre Jülich, 52425 Jülich, Germany. [2] Department of Physics and JILA, University of Colorado and NIST, Boulder, Colorado, USA. [3] Department of Physics and Astronomy, Uppsala University, SE-75120 Uppsala, Sweden. [4] Electromagnetics Division, National Institute of Standards and Technology, Boulder, Colorado, USA. [5] University of Kaiserslautern and Research Center OPTIMAS, 67663 Kaiserslautern, Germany. *These authors contributed equally to this work. Correspondence and requests for materials should be addressed to R.A. (email: r.adam@fz-juelich.de).

One of the major roadblocks for continued progress in nanoelectronics is energy dissipation caused by the flow of electrical current. Encoding data in electron spin, rather than charge, promises a new route for technology with the potential to dramatically reduce these energy requirements. A current grand challenge in this area is to control the static and dynamic behaviour of spins and spin ensembles. Spin dynamics is in-itself of fundamental interest for understanding spin–photon–charge–phonon interactions and their complex interplay on femtosecond to picosecond timescales. The potential to rapidly manipulate spins was first demonstrated in a pioneering experiment[1] on Ni that observed that the magnetization of 3*d* ferromagnets can be optically quenched within 50–300 fs after excitation by a femtosecond laser pulse[2,3]. This ultrafast demagnetization is then followed by a slower magnetization recovery on picosecond timescales. Optically induced magnetization reversal has also been demonstrated using circularly polarized light[4]. A number of distinct models have been proposed to describe how laser excitation can couple so quickly to the spins, given that the light itself does not directly exert a significant torque on the electron spins. Most of these models are based on phonon-, electron- and magnon-mediated spin–flip processes[5–9], direct laser-induced spin–flips[10] or relativistic spin–light interaction[11]. Most recently, a new model based on superdiffusive spin transport has been proposed[12,13].

The variety of these distinct interpretations suggests that several physical mechanisms may govern femtosecond spin dynamics even in a simple elemental magnet. The physics becomes even more intriguing for heterogeneous magnetic systems, such as magnetic compounds[14], alloys[15,16] and exchange-coupled layered structures. Several sophisticated experiments have recently employed ultrashort soft X-ray pulses from synchrotron[2,15] or laser-driven high-harmonic (HHG) light sources[3,16,17] to disentangle the various processes using element-specific demagnetization techniques. This has been achieved by monitoring the absorption or reflection of light tuned to inner-shell absorption edges of magnetic materials. Using these new capabilities, unexpected new spin dynamics can be uncovered—for example, even in a strongly coupled ferromagnetic permalloy ($Fe_{20}Ni_{80}$), the magnetization of Fe quenches faster than the Ni magnetization for a time shorter than the characteristic energy/time equivalent of the exchange coupling energy of the alloy[16]. In magnetic multilayers, magnetization dynamics has been previously studied on nanosecond to picosecond timescales[18–20]. However, accurately explaining how multilayer systems demagnetize on femtosecond timescales has proven challenging. Recent exciting experiments optically pumped layered magnetic structures using femtosecond lasers[21,22] and inferred the resulting spin transport dynamics using visible probe light.

Here we exploit the combination of simple magnetic multilayer structures and the powerful capability of our HHG probe to simultaneously monitor layer-specific magnetization dynamics. We study a Ni/Ru/Fe trilayer stack under conditions where superdiffusive spin transport is the dominant process determining spin dynamics on the fastest timescales. By optically exciting the stack with femtosecond laser pulses and probing the resulting magnetization dynamics in the Ni and Fe layers simultaneously but element-selectively at the 3*p* (M) absorption edges of Ni (66 eV) and Fe (52 eV), we directly observe magnetization dynamics in individual layers. Remarkably, we find that the femtosecond spin dynamics of the individual Ni and Fe layers depends on the relative alignment of their initial magnetization directions: ultrafast excitation and demagnetization of the Ni layer transiently enhances the magnetization of the buried Fe layer when their magnetizations are initially aligned parallel to each other, whereas the magnetization of the Fe layer decreases if its initial magnetization is antiparallel to that of Ni. These findings can be explained consistently by large laser-generated superdiffusive spin currents[12,13]. In this physical picture, superdiffusion of excited spin

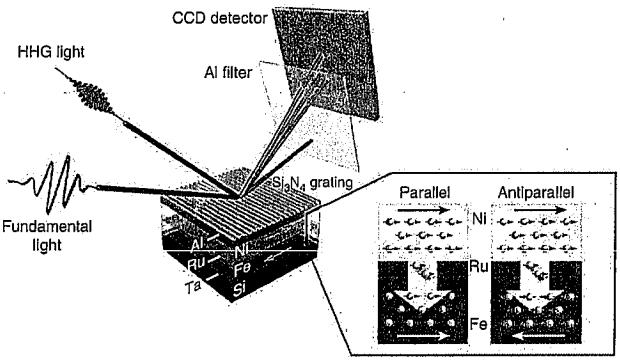

Figure 1 | Experimental setup and the multilayer sample schematics. The magnetization of the Al/Ni/Ru/Fe multilayer samples is probed by XUV high harmonics at the 3*p* absorption edges of Fe and Ni. The Si_3N_4 grating on top of the layers spectrally separates the XUV high harmonic beams that are then detected by an X-ray CCD detector. The pump laser light absorbed in the thin Al and Ni layers results in a spin current (marked by grey arrow in the inset) that travels through the non-magnetic Ru spacer layer into the Fe layer. The magnetization of the Fe layer increases or decreases depending on its orientation relative to Ni. The inset illustrates schematically the relative magnetization of the Ni and Fe layers (thin black and white arrows), the majority spin alignment in the layers (red and green circles) and the flow of the spin current (large grey arrow).

majority electrons from the Ni layer, through the Ru layer and into the buried Fe layer can transiently increase or decrease the magnetization in Fe depending on its relative spin alignment with respect to Ni (which can be controlled by the external magnetic field and the thickness of the Ru spacer layer).

Results

Multilayer fabrication and characterization. Our samples consist of Al(3 nm)/Ni(5 nm)/Ru(x)/Fe(4 nm)/Ta(3 nm) layers (see Methods), where the Ni/Ru/Fe trilayer forms an interlayer exchange-coupled magnetic system (Fig. 1). The top Si_3N_4 grating structure serves as a grating spectrometer to spectrally disperse the extreme ultraviolet (XUV) HHG radiation spanning from approximately 20 to 72 eV. The magnetism in our samples was carefully characterized using a superconducting quantum interference device (SQUID) magnetometer. These data (see Fig. 2) show the influence of the Ru spacer thickness on the interlayer exchange-coupling between Ni and Fe layers: a 1 nm thick Ru layer results in a ground-state ferromagnetic coupling for Ni and Fe, which changes to antiferromagnetic coupling for a 1.5 nm Ru layer thickness.

Static magnetic asymmetry. The magneto-optical response of our trilayers is measured via the transverse magneto-optical Kerr effect (T-MOKE) in XUV spectral range[23–25] (see Supplementary Methods for a more detailed description). Magnetic asymmetry can be defined as

$$A = \frac{I_r(H^{\uparrow}) - I_r(H^{\downarrow})}{I_r(H^{\uparrow}) + I_r(H^{\downarrow})} \quad (1)$$

where $I_r(H^{\uparrow})$ and $I_r(H^{\downarrow})$ denote the intensities of the reflected light as the externally applied magnetic field H is reversed in direction. Measuring $I_r(H)$ for these two opposite field directions gives an artifact-free and sensitive measurement of the magnetic state[16,17,26]. The resonantly enhanced static magnetic asymmetry at the Fe and Ni 3*p* absorption edges (52 and 66 eV, respectively) can be clearly assigned to the magnetic state of the Fe and Ni layers, as shown in Fig. 3. For our Ni/Ru/Fe trilayer, the amplitude of the magnetic asymmetry is

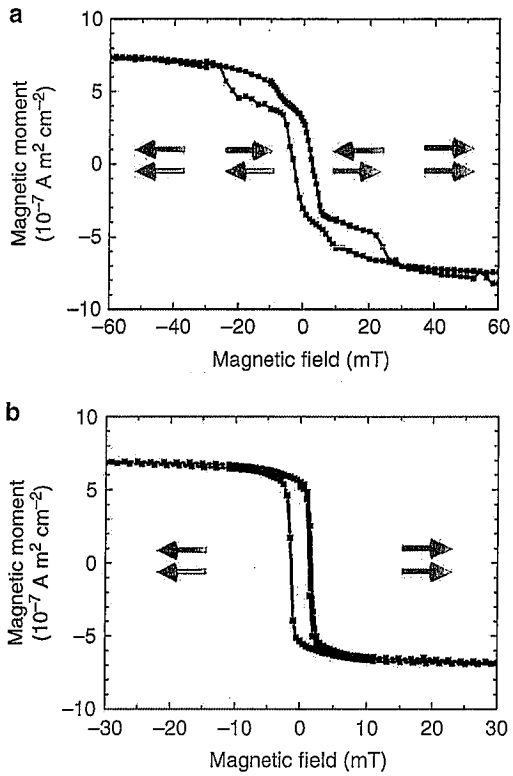

Figure 2 | Magnetic hysteresis loops. The magnetic moment of the Ni(5 nm)/Ru(x)/Fe(4 nm) trilayers, where $x = 1$ nm and 1.5 nm, was measured by a SQUID magnetometer at 290 K. The Fe and Ni layers in the trilayer with a Ru thickness of 1.5 nm (**a**) are antiferromagnetically coupled in zero external magnetic field, whereas they are ferromagnetically coupled in the 1 nm thick Ru trilayer (**b**). The red and blue arrows show the magnetizations of Fe (red) and Ni (blue) layers indicating the relative magnetization orientation within a specific magnetic field range.

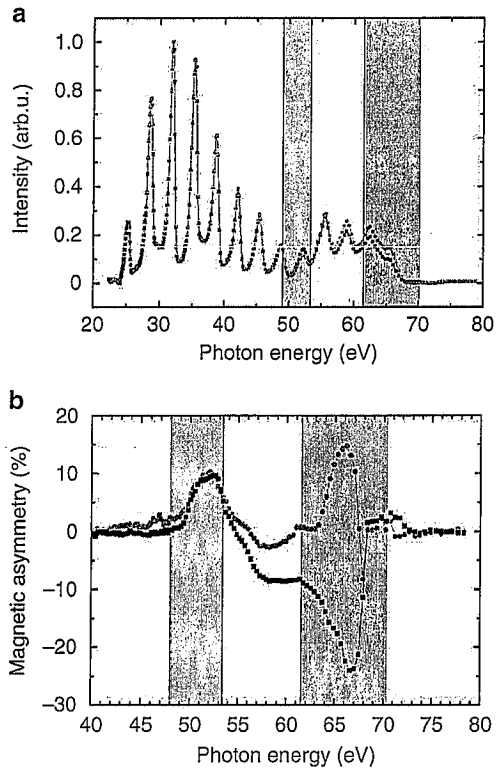

Figure 3 | High harmonics and magnetic asymmetry spectra. (**a**) Spectra of high harmonics reflected from the sample depend on the orientation of the external magnetic field ($H^{\uparrow}$ or $H^{\downarrow}$). The spectra are taken for parallel alignment of the Ni and Fe magnetizations for $H^{\uparrow}$ (black squares) and $H^{\downarrow}$ (grey circles). The spectra differ at the 3*p* absorption edges of Ni (blue-coloured area) and Fe (red-coloured area). (**b**) Fe and Ni magnetic contributions can be separated in the magnetic asymmetry calculated from high harmonics spectra (equation (1)). The 3*p* absorption edges of Fe and Ni are marked by red- and blue-coloured areas. For parallel alignment of the Ni and Fe magnetizations the Ni and Fe asymmetry peaks have different signs (black squares) whereas for the antiparallel alignment (red circles) the sign of the Ni asymmetry peak reverses.

around 10% at the Fe absorption edge and 20% at the Ni 3*p* edge. By adjusting the external magnetic field from 0 to ±60 mT, we can tune the trilayers into two well-defined magnetic states: one with parallel orientation of the Ni and Fe magnetizations and one with antiparallel orientation. A comparison of the magnetic asymmetries corresponding to the two states shows that the relative sign of the Ni and Fe asymmetries reverses in these two cases.

Magnetization dynamics. To capture spin transport and magnetization dynamics in our trilayer, the samples are excited with femtosecond pump laser pulses of 1.6 eV photon energy. The magnetization in the individual layers was then captured simultaneously by monitoring the amplitude of the T-MOKE magnetic asymmetry as a function of time delay. To estimate the amount of the pump light reaching the individual layers, we performed a self-consistent 2×2 matrix calculation of the optical properties for the full metallic layer stack for our experimental conditions. We find that the combination of the Al cap and Ni layer together absorbs >58% of the incident light—about 2.5 times as much as the Fe layer. Generally, as in all optical pump-probe experiments, it is possible that the magneto-optical signal is affected by the hot electrons, in which case the signal would also change sign with switching the magnetization. However, the fact that changing the relative magnetization direction of the Fe layer relative to the Ni layer (see below) causes an increase or decrease of the observed Fe magnetization, rules out such measurement artifacts. In addition, in a previous publication[17] we showed that the nonmagnetic contribution to the asymmetry parameter is small (0.2%) compared with the amplitude of demagnetization (20%), demonstrating that XUV T-MOKE can sensitively probe element-selective spin dynamics.

The layer-selective time traces of the magnetic asymmetries at the 3*p* absorption edges of Fe and Ni, at fluencies of $F \approx 2$ mJ cm^{-2}, are plotted in Fig. 4a,b. Similar to earlier experiments[1,2,3,5], we observe a magnetization quenching in the Ni layer of the stack. Surprisingly, however, we also observe either an enhancement or reduction of the Fe magnetization depending on the relative magnetization orientation of the Ni and Fe layers (see Fig. 4a,b): if the Fe and Ni layers are initially oriented antiparallel, then the magnetization of both Ni and Fe decreases. On the other hand, if the two layers are oriented parallel by an external magnetic field, we observe that the Fe magnetization increases 15% above its equilibrium value on a similar timescale. In a second layer stack with Ni(5 nm)/Ru(1 nm)/Fe(4 nm), where the Ni magnetization only aligns parallel to the Fe one (Fig. 4c), we observe again an enhancement in the Fe magnetization after laser excitation.

Superdiffusive spin transport. This first observation of an ultrafast magnetization enhancement in the Fe layer can be explained by superdiffusive spin transport[12,13] (see also Supplementary Discussion), taking place on timescales comparable to the demagnetization

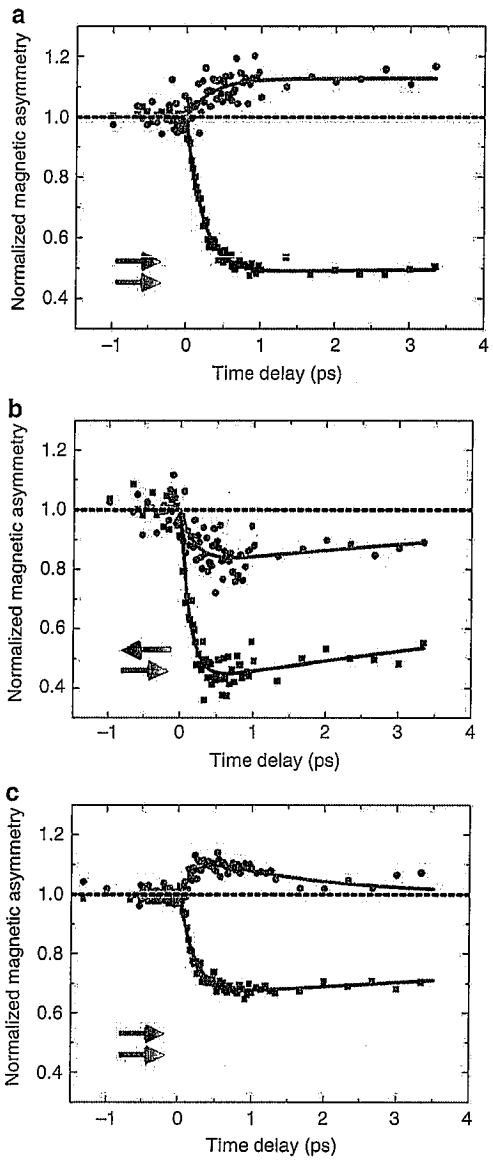

Figure 4 | Experimentally measured time- and layer-resolved magnetization. The time-resolved magnetization of the Fe and Ni layers in the Ni(5 nm)/Ru(1.5 nm)/Fe(4 nm) trilayer for the parallel (**a**) and antiparallel (**b**) magnetization alignment and in the Ni(5 nm)/Ru(1 nm)/Fe(4 nm) trilayer (**c**) for the parallel magnetization alignment. The data have been extracted by integrating the magnetic asymmetry signal over the 3*p* absorption edges of Fe and Ni, as indicated by the red- and blue-coloured areas in Fig. 3, respectively, and normalizing to the magnetic asymmetry values before the time zero (black broken line). The magnetic asymmetry at the Fe 3*p* absorption edge anomalously increases for the parallel (**a**,**c**) and decreases for antiparallel magnetic orientation of Ni and Fe layers (**b**). For the Ni(5 nm)/Ru(1 nm)/Fe(4 nm) trilayer, only parallel magnetization orientation is possible due to ferromagnetic coupling. The curves are least square fits to Supplementary Equation (S2).

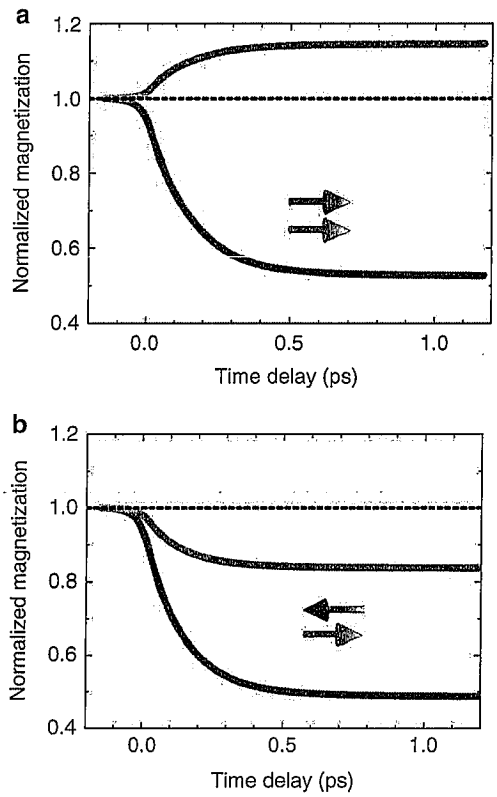

Figure 5 | Calculated time- and layer-resolved magnetization. In our model, laser-induced ultrafast demagnetization of the Ni layer (blue curves in (**a**) and (**b**)) generates superdiffusive spin currents that increase the Fe magnetization for parallel orientation (**a**) (red curve), whereas decreasing the Fe magnetization for antiparallel alignment (**b**) (red curve). The strengths and timescales of demagnetization and magnetization agree well with the measured data.

processes explored in earlier works[1–3,5]. The mechanism we propose for enhancement of the magnetization is based on filling of majority spin states above the Fermi energy in the Fe layer by majority spins coming from Ni. This leads to a transient magnetization increase in the Fe layer, above its maximum value defined by the Curie curve at $T=0$ K. The increase in the magnetic signal from the Fe layer is a result of a strong asymmetry in the spin-dependent hot-electron lifetimes in magnetic materials and, hence, the transport properties of the hot majority and minority spin carriers[27–29] within the Ni and Fe layers. Excited minority spin electrons originating in the optical excitation in both the Al and Ni layers have much shorter lifetimes when passing via superdiffusion through the Ni layer, and are therefore stopped before they can reach the Fe layer. Conversely, majority-spin electrons have much longer lifetimes in Ni and are able to reach the Fe layer by superdiffusion. Solving the superdiffusion spin-transport equation (see Methods) for electrons excited by a laser pulse of 25 fs and 1.6 eV photon energy in the Al, Ni and Fe layers, we predict the transient, layer-specific, normalized magnetizations shown in Fig. 5. The transient response of the Fe layer depends strikingly on the initial relative alignment of the Ni and Fe layers: for antiparallel magnetization alignment, the stream of spin-majority electrons decreases the net magnetization in the Fe layer by increasing the amount of spin-minority electrons in Fe. Conversely, for parallel configuration, the superdiffusive spin current of spin majority electrons through the interface increases the number of spin-majority electrons in Fe, thus increasing the net Fe magnetization and causing opposite polarities in the femtosecond magnetization response of Ni and Fe layers.

Discussion

Several competing processes have been proposed for magnetization dynamics on ultrafast timescales[5–13]. For the trilayer systems explored here, we find that the observed magnetization dynamics in the Ni and buried Fe layer is consistent with superdiffusion of

excited spin-majority electrons that originate in the Al and Ni layers. The experimental data (Fig. 4a,b) agree well with theoretical predictions of superdiffusive spin transport (Fig. 5a,b)–both in terms of the timescales as well as the magnitudes of the demagnetization (~15% for Fe and ~50% for Ni) and anomalous magnetization increase in Fe (~15%). We note that we have not included spin dissipation channels such as electron–phonon[5] and electron–electron[7] spin–flip scattering in our model. This excellent agreement between theory and experiment thus shows that superdiffusion is the dominant process for the observed spin dynamics in the Ni and Fe layers under the chosen experimental conditions.

The anomalous enhancement of the Fe magnetization is most prominent at relatively low excitation fluence, below $F \approx 2.0\,\mathrm{mJ\,cm^{-2}}$. We find that at higher fluence, direct optical excitation of the Fe layer becomes the dominant source of demagnetization, that is, by increasing the excitation fluence to $F \approx 2.7\,\mathrm{mJ\,cm^{-2}}$, we observe the Fe magnetization to decrease after excitation, even when the Ni and Fe magnetizations are parallel (see Supplementary Fig. S2). This observation confirms theoretical predictions that the superdiffusive spin current saturates at high excitation powers[12,13]. Conversely, when we reduce the pump fluence to $F \approx 1.3\,\mathrm{mJ\,cm^{-2}}$, we again observe an increase or decrease of magnetization in Fe due to superdiffusive spin transfer, though the effect is weaker than the response shown in Fig. 4.

In summary, by probing ultrafast spin dynamics in interlayer exchange-coupled magnetic structures with elemental specificity using broad bandwidth coherent high harmonic radiation, we are able to elucidate the contribution of spin superdiffusion to the process of ultrafast spin dynamics. Spin superdiffusion leads to a remarkable and counterintuitive magnetization enhancement in Fe in response to optical pumping when the Ni and Fe magnetizations are initially parallel. Our discovery provides fundamental insight into spin dynamics on femtosecond timescales, and is relevant for identifying the mechanisms underlying ultrafast spin dynamics. We note that our data demonstrate an ultrafast transfer of angular momentum of longitudinal spin through a spin current on subpicosecond timescales. In contrast, previous works demonstrated spin-transfer torque, that is, a transfer of transverse angular momentum between noncollinear spins and a magnetic moment at microwave frequencies[30–33], leading to important innovations such as spin–torque magnetic random access memory (RAM) for data storage, spin–torque oscillators for frequency-agile telecommunications, and spin–wave interconnects for spin-based logic. Similarly, we anticipate that superdiffusive spin transfer, which has a considerably larger magnetic moment, can find applications in moving domain walls, switching magnetic nano-elements on subpicosecond timescales or in spin-based electronics operating in the Terahertz frequency range.

Methods

Sample fabrication and experiment. The Al(3 nm)/Ni(5 nm)/Ru(x)/Fe(4 nm)/Ta(3 nm) multilayers (Al on top) with two different Ru thicknesses $x = 1$ nm and 1.5 nm were fabricated on Si substrates by use of ion beam sputtering. To ensure proper crystal texture, samples were grown on top of a thin Ta layer. Al capping layer prevents oxidation of the magnetic layers. The Al is self-passivating, and we expect that the top layer actually consists of approximately 1.5 nm of AlO_x that covers 2 nm of metallic Al. The entire structure is sufficiently thin for the XUV light to penetrate through and probe the magnetization of the Fe layer. To generate laser high-order harmonics in the XUV, we used a laser amplifier generating laser pulses with 25 fs duration, 1.9 mJ energy and 1.6 eV photon energy, at 3 kHz repetition rate. Ninety percent of the laser power was focused into a Ne-filled capillary with 150 μm diameter to generate HHG spanning 20–72 eV (ref. 34), whereas 10% of the laser energy is used to excite the sample with femtosecond laser pulses with fluencies of, approximately, $2\,\mathrm{mJ\,cm^{-2}}$. The estimated duration of the XUV pulses is < 10 fs (ref. 16), and the XUV light was focused onto the sample using a grazing incidence toroidal mirror. The sample was aligned in the T-MOKE geometry with the magnetization vector of the sample perpendicular to the plane of incidence (see Supplementary Methods). The p-polarized XUV probe light is reflected at an angle of 45° with respect to the sample surface. The XUV photon energy calibration was performed using the Al filter that serves to shield the CCD (charge-coupled device) detector from direct laser light, and has a well-defined absorption edge at 72.6 eV.

Theoretical model and calculations. The calculations are based on the superdiffusive spin transport equation[12,13],

$$\frac{\partial n(\sigma,E,z,t)}{\partial t} + \frac{n(\sigma,E,z,t)}{\tau(\sigma,E,z)} = \left(-\frac{\partial}{\partial z}\hat{\phi} + \hat{I}\right) \times \left(\hat{S}n(\sigma,E,z,t) + S^{\mathrm{ext}}(\sigma,E,z,t)\right) \quad (2)$$

where $n(\sigma, E, z, t)$ is the spin- and energy-dependent density of laser-excited electrons, $\tau(\sigma, E, z)$ is the lifetime, $\hat{\phi}$ and $\hat{I}$ are the electron flux and identity operators, $\hat{S}$ is an integral operator that computes the source term for next-generation electrons, which result from elastic, inelastic, as well as cascade processes, and $S^{\mathrm{ext}}(\sigma, E, z, t)$ is the source term containing explicitly the 25 fs pump pulse. The z coordinate is defined as being normal to the layers. The spin- and excitation energy-dependent electronic lifetimes and velocities[27,29], as well as the ratio of excited majority to minority spin electrons[35], are taken from *ab initio* calculations. The femtosecond spin dynamics follows from $m(E, z, t) = 2\mu_B[n(\uparrow, E, z, t) - n(\downarrow, E, z, t)]$, with $m(E, z, t)$ the transient spin moment of excited electrons along the depth profile. The material-dependent $M(t)$ is computed as the energy-integrated average of $m(E, z, t)$ over an individual layer.

Partial reflection at the interfaces between two layers has been included. The energy- and spin-dependent reflectivity has been computed assuming the electrons cross the interface as classical particles, with velocity defined by the band structure in each material. The reflected fraction has been obtained by requiring the conservation of linear momentum upon crossing of the interface. All possible multiple reflection paths are taken rigorously into account.

In the calculations of Fig. 5, we assumed a 5 nm Ni and 4 nm Fe layer with a 3 nm Al capping layer; however, the Ru layer was not included. The Ru layer, being thin and embedded between the two ferromagnetic layers, will have a spin lifetime and velocity different from those of bulk Ru, therefore, the parameters of this thin Ru layer are not well known. However, as the Ru layer is very thin, it has only a marginal role in the transport and can to a good approximation be neglected.

References

1. Beaurepaire, E., Merle, J.- C., Daunois, A. & Bigot, J.- Y. Ultrafast spin dynamics in ferromagnetic nickel. *Phys. Rev. Lett.* **76**, 4250–4253 (1996).
2. Stamm, C. *et al.* Femtosecond modification of electron localization and transfer of angular momentum in nickel. *Nat. Mater.* **6**, 740–743 (2007).
3. La-O-Vorakiat, C. *et al.* Ultrafast soft x-ray magneto-optics at the *M*-edge using a tabletop high-harmonic source. *Phys. Rev. Lett.* **103**, 257402 (2009).
4. Stanciu, C. D. *et al.* All-optical magnetic recording with circularly polarized light. *Phys. Rev. Lett.* **99**, 047601 (2007).
5. Koopmans, B. *et al.* Explaining the paradoxical diversity of ultrafast laser-induced demagnetization. *Nat. Mater.* **9**, 259–265 (2010).
6. Carva, K., Battiato, M. & Oppeneer, P. M. Ab initio investigation of the Elliott-Yafet electron-phonon mechanism in laser-induced ultrafast demagnetization. *Phys. Rev. Lett.* **107**, 207201 (2011).
7. Krauß, M. *et al.* Ultrafast demagnetization of ferromagnetic transition metals: the role of the Coulomb interaction. *Phys. Rev. B* **80**, 180407 (2009).
8. Mueller, B. Y., Roth, T., Cinchetti, M., Aeschlimann, M. & Rethfeld, B. Driving force of ultrafast magnetization dynamics. *New J. Phys.* **13**, 123010 (2011).
9. Carpene, E. *et al.* Dynamics of electron-magnon interaction and ultrafast demagnetization in thin iron films. *Phys. Rev. B* **78**, 174422 (2008).
10. Zhang, G. P., Hübner, W., Lefkidis, G., Bai, Y. & George, T. F. Paradigm of the time-resolved magneto-optical Kerr effect for femtosecond magnetism. *Nat. Phys.* **5**, 499–502 (2009).
11. Bigot, J.- Y., Vomir, M. & Beaurepaire, E. Coherent ultrafast magnetism induced by femtosecond laser pulses. *Nat. Phys.* **5**, 515–520 (2009).
12. Battiato, M., Carva, K. & Oppeneer, P. M. Superdiffusive spin transport as a mechanism of ultrafast demagnetization. *Phys. Rev. Lett.* **105**, 027203 (2010).
13. Battiato, M., Carva, K. & Oppeneer, P. M. Theory of laser-induced ultrafast superdiffusive spin transport in layered heterostructures. *Phys. Rev. B* **86**, 024404 (2012).
14. Müller, G. M. *et al.* Spin-polarization in half-metals probed by femtosecond spin excitation. *Nat. Mater.* **8**, 56–61 (2009).
15. Radu, I. *et al.* Transient ferromagnetic-like state mediating ultrafast reversal of antiferromagnetically coupled spins. *Nature* **472**, 205–208 (2011).
16. Mathias, S. *et al.* Probing the timescale of the exchange interaction in a ferromagnetic alloy. *P. Natl Acad. Sci. USA* **109**, 4792–4797 (2012).
17. La-O-Vorakiat, C. *et al.* Ultrafast demagnetization measurements using extreme ultraviolet light: comparison of electronic and magnetic contributions. *Phys. Rev. X* **2**, 011005 (2012).
18. Adam, R., Grychtol, P., Cramm, S. & Schneider, C. M. Time-resolved measurements of $Ni_{80}Fe_{20}$/MgO/Co trilayers in the extreme ultraviolet range. *J. Electron Spectrosc. Relat. Phenomena* **184**, 291–295 (2011).

19. Ju, G. *et al.* Ultrafast time resolved photoinduced magnetization rotation in a ferromagnetic/antiferromagnetic exchange coupled system. *Phys. Rev. Lett.* **82,** 3705–3708 (1999).
20. Kaiser, A. M., Wiemann, C., Cramm, S. & Schneider, C. M. Spatially resolved observation of uniform precession modes in spin-valve systems. *J. Appl. Phys.* **109,** 07D305 (2011).
21. Melnikov, A. *et al.* Ultrafast transport of laser-excited spin-polarized carriers in Au/Fe/MgO(001). *Phys. Rev. Lett.* **107,** 076601 (2011).
22. Malinowski, G. *et al.* Control of speed and efficiency of ultrafast demagnetization by direct transfer of spin angular momentum. *Nat. Phys.* **4,** 855–858 (2008).
23. Hecker, M., Oppeneer, P. M., Valencia, S., Mertins, H.-Ch. & Schneider, C. M. Soft X-ray magnetic reflection spectroscopy at the 3*p* absorption edges of thin Fe films. *J. Electron Spectrosc. Rel. Phenomena* **144–147,** 881–884 (2005).
24. Grychtol, P. *et al.* Resonant magnetic reflectivity in the extreme ultraviolet spectral range: interlayer-coupled Co/Si/Ni/Fe multilayer system. *Phys. Rev. B* **82,** 054433 (2010).
25. Grychtol, P. *et al.* Layer-selective studies of an anti-ferromagnetically coupled multilayer by resonant magnetic reflectivity in the extreme ultraviolet range. *J. Electron Spectrosc. Rel. Phenomena* **184,** 287–290 (2011).
26. Bigot, J.- V. Spin-sensitive optics. *Physics* **5,** 11 (2012).
27. Zhukov, V. P., Chulkov, E. V. & Echenique, P. M. GW+T theory of excited electron lifetimes in metals. *Phys. Rev. B* **72,** 155109 (2005).
28. Aeschlimann, M. *et al.* Ultrafast spin-dependent electron dynamics in fcc Co. *Phys. Rev. Lett.* **79,** 5158–5161 (1997).
29. Zhukov, V. P., Chulkov, E. V. & Echenique, P. M. Lifetimes and inelastic mean free path of low-energy excited electrons in Fe, Ni, Pt, and Au: Ab initio GW+T calculations. *Phys. Rev. B* **73,** 125105 (2006).
30. Myers, E. B., Ralph, D. C., Katine, J. A., Louie, R. N. & Buhrman, R. A. Current-induced switching of domains in magnetic multilayer devices. *Science* **285,** 867–870 (1999).
31. Tserkovnyak, Y., Brataas, A., Bauer, G. E. W. & Halperin, B. I. Nonlocal magnetization dynamics in ferromagnetic heterostructures. *Rev. Mod. Phys.* **77,** 1375–1421 (2005).
32. Costache, M. V., Sladkov, M., Watts, S. M., van der Wal, C. H. & van Wees, B. J. Electrical detection of spin pumping due to the precessing magnetization of a single ferromagnet. *Phys. Rev. Lett.* **97,** 216603 (2006).
33. Woltersdorf, G., Mosendz, O., Heinrich, B. & Back, C. H. Magnetization dynamics due to pure spin currents in magnetic double layers. *Phys. Rev. Lett.* **99,** 246603 (2007).
34. Kapteyn, H. C., Murnane, M. M. & Christov, I. P. Extreme nonlinear optics: coherent X-rays from lasers. *Phys. Today* **58,** 39–46 (2005).
35. Oppeneer, P. M. & Liebsch, A. Ultrafast demagnetization in Ni: theory of magneto-optics for non-equilibrium electron distributions. *J. Phys. Condens. Matter* **16,** 5519–5530 (2004).

Acknowledgements

The experimental work was funded by the X-Ray Scattering Program of the U.S. Department of Energy Office of Basic Energy Science, and made use of facilities provided by the NSF Engineering Research Center in EUV Science and Technology. Financial support by the Swedish Research Council (VR), the European Community's Seventh Framework Programme (FP7/2007-2013) under grant agreement No. 214810, (FANTOMAS), grant agreement No. GA 253316 (International Outgoing Fellowship, S.M.), and the Swedish National Infrastructure for Computing (SNIC) is gratefully acknowledged. We would like to thank Jürgen Lauer, Bernd Küpper, Heinz Pfeifer, Konrad Bickmann and Thomas Jansen for technical support and Bastian Heller for SQUID measurements. We thank Ben Langdon and Neil Anderson at KMLabs Inc. for technical support and Karel Carva and Mirko Cinchetti for discussions.

Author contributions

D.R., C.L., and M.B. contributed equally to this work, D.R., C.L., E.T. carried out the experiments and data analysis, M.B., P.M., P.M.O. developed the theoretical explanation and performed simulations, R.A., P.G., J.M.S. designed the multilayers and discussed the results, J.M.S. fabricated the samples, C.L., S.M., P.G., R.A., H.C.K., M.M.M. developed the experimental setup and discussed the results, M.B., T.J.S., H.T.N., E.T. calculated the light absorption in the multilayer and discussed the results, M.A., H.C.K., M.M.M., C.M.S., M.B., P.M.O. contributed to the manuscript writing and discussion of results. All co-authors contributed to the data interpretation, internal discussion and the manuscript writing.

Additional information

Supplementary Information accompanies this paper at http://www.nature.com/naturecommunications

Competing financial interests: The authors declare no competing financial interests.

Reprints and permission information is available online at http://npg.nature.com/reprintsandpermissions/

How to cite this article: Rudolf, D. *et al.* Ultrafast magnetization enhancement in metallic multilayers driven by superdiffusive spin current. *Nat. Commun.* 3:1037 doi: 10.1038/ncomms2029 (2012).

Supplementary Information for Ultrafast magnetization enhancement in metallic multilayers driven by superdiffusive spin current

Dennis Rudolf,[1*] Chan La-O-Vorakiat,[2*] Marco Battiato,[3*] Roman Adam,[1] Justin M. Shaw,[4] Emrah Turgut,[2] Pablo Maldonado,[3] Stefan Mathias,[2,5] Patrik Grychtol,[1,2] Hans T. Nembach,[4] Thomas J. Silva,[4] Martin Aeschlimann,[5] Henry C. Kapteyn,[2] Margaret M. Murnane,[2] Claus M. Schneider[1] and Peter M. Oppeneer[3]

[1]*Peter Grünberg Institut PGI-6 & JARA-FIT, Research Centre Jülich, 52425 Jülich, Germany*
[2]*Department of Physics and JILA, University of Colorado and NIST, Boulder, CO, USA*
[3]*Department of Physics and Astronomy, Uppsala University, SE-75120 Uppsala, Sweden*
[4]*Electromagnetics Division, National Institute of Standards and Technology, Boulder, CO, USA*
[5]*University of Kaiserslautern and Research Center OPTIMAS, 67663 Kaiserslautern, Germany*

Corresponding author: r.adam@fz-juelich.de

SUPPLEMENTARY FIGURES

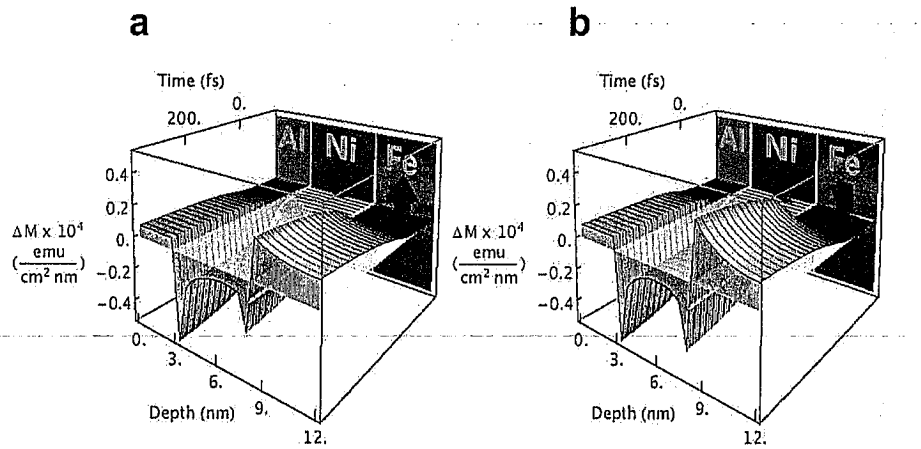

Supplementary Figure S1| Evolution of the trilayer magnetization in space and time. The magnetization change ΔM compared to the case of thermal equilibrium in a trilayer consisting of Al, Ni and Fe layers is displayed for parallel **(a)** and antiparallel **(b)** magnetization alignment within the first 500 fs after laser excitation along the depth profile of the layers. The Ni spin-majority electrons move by superdiffusion predominantly from the interface region into the Fe and Al layers, thus decreasing the Ni magnetization.

* These authors contributed equally to this work.

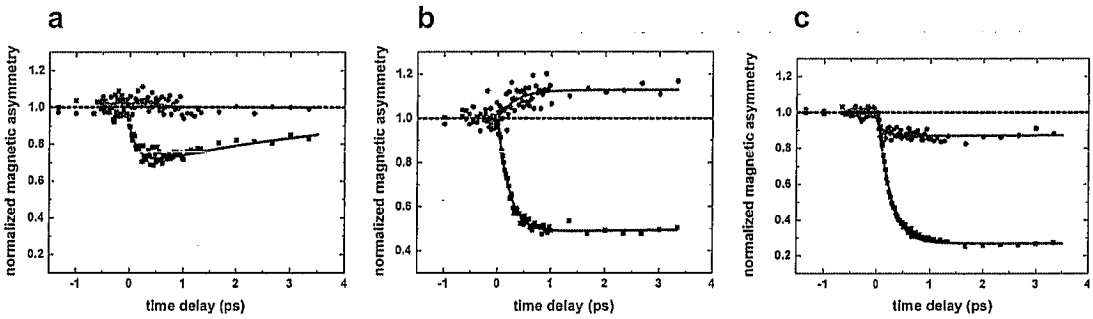

Supplementary Figure S2| Fluence-dependent time- and layer- resolved magnetization. The effect of the superdiffusive spin-transfer current on the magnetization dynamics of the Fe layer can only be observed if other demagnetization channels are small in comparison. By measuring the laser fluence dependence of the spin dynamics for *parallel* magnetization alignment of the Ni and Fe layers, we identified the optimal conditions for observing a magnetization enhancement due to superdiffusive spin currents reaching the Fe layer. Experimentally, for laser pump fluences of 1.3 mJ/cm^2, there is a weak transient enhancement of the Fe magnetization for parallel Fe/Ni magnetization alignment **(a)**. When the laser fluence is increased to 2.0 mJ/cm^2, we observe the strongest *magnetization enhancement* **(b)**. For an even higher fluence of 2.7 mJ/cm^2, we observe the onset of an additional demagnetization channel in Fe, which acts in the opposite direction to the superdiffusive spin-transfer from the Ni and the magnetization in the Fe layer displays ultrafast *demagnetization* **(c)**. Such behavior is consistent with the expectation that the generation of superdiffusive spin currents in the top Al/Ni layers saturates at the laser pump fluence between 2.0 and 2.7 mJ/cm^2.

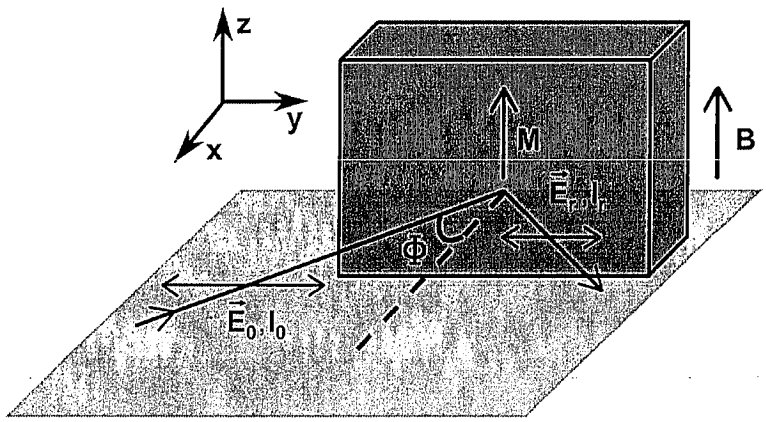

Supplementary Figure S3| Geometry of the transverse magneto-optical Kerr effect (T-MOKE). The amplitude of the incident electric field E_0 linearly polarized in the x-y-plane penetrating the sample at angle Φ is changed by the magnitude and the direction of the sample magnetization M pointing in the z-direction perpendicular to the plane of incidence. Thus, the reflected electric field amplitude E_r and the intensity I_r depend on M.

SUPPLEMENTARY TABLE

	τ_m (in fs)		τ_r (in ps)	
	↑↑	↑↓	↑↑	↑↓
Ni(5 nm)/Ru(1.5 nm)/Fe(4 nm)	219 ±19	136±24	> 200	15±10
Ni(5 nm)/Ru(1 nm)/Fe(4 nm)	208±33		22±17	

Supplementary Table S1| Demagnetization (τ_m) and remagnetization (τ_r) times. The relevant values were obtained from time-resolved T-MOKE magnetic asymmetry measurements integrating over the Ni 3p absorption edge (around 66 eV) for parallel and antiparallel magnetization orientation of the Ni and Fe layers. A phenomenological exponential equation, Supplementary Equation S2, is used to extract the time parameters.

SUPPLEMENTARY DISCUSSION

Superdiffusive spin transport theory was used to describe the dynamics of ultrafast, non-equilibrium, laser-excited electrons[12,13] in magnetic multilayers. The governing equation Eq. (2) (see Methods in the main text) provides a geometrically exact kinematic description of the excited electron transport on femtosecond timescales. It therefore models accurately the laser-generated spin-polarized electron transport, which is essential since excited electron lifetimes in ferromagnetic *3d*-metals like Ni and Fe are of the order of a few tens of femtoseconds, while the mean-free-paths are on the order of the thickness of the layered structure. Therefore, commonly adopted transport approximations such as ballistic or standard diffusion models cannot be used.

Superdiffusion-driven magnetization dynamics can be viewed as arising from two main effects. One important contribution to the magnetization dynamics originates from the interface between two different materials, as pointed out in the previous publications [12,13], where the transport properties change abruptly, thereby resulting in regions of spin accumulation. A second contribution is due to volumetric spin depletion in an optically excited layer.

The theoretical demagnetization times τ_M can be obtained by fitting the computed element-specific $\Delta M(t)$ curves in Figure 5 of the main text with Supplementary Equation S2. This gives τ_M = 148±10 fs for both parallel and antiparallel alignment of Ni with respect to the Fe layers. We predict essentially the same values for the Fe demagnetization time in an antiparallel geometry with respect to Ni, and for the Fe anomalous magnetization increase in a parallel geometry. Comparable demagnetization times are also extracted from the experimental data (Supplementary Table S1).

In Supplementary Figures S1a and S1b, we report the computed position- and time-dependent changes in the magnetization, i.e. $\Delta M(z,t)$, of the Al/Ni/Fe layers, calculated as the superposition of the transport of spin up and down electrons (see Supplementary Methods). The *z*-coordinate is defined as perpendicular to the layers, starting at the Al surface. The values for the static magnetization used for Ni and Fe are $0.38\ 10^{-4}$ emu/(cm^2 nm) and $1.39\ 10^{-4}$ emu/(cm^2 nm), respectively. The resulting magnetization change profiles look similar for the parallel and antiparallel alignment of Ni and Fe films. They are not similar in fact, but appear to be because the transport properties of non-equilibrium electrons in Fe are poorer and have a lower spin asymmetry than those in Ni.

Let us consider in more detail the laser-induced spin transport. First, superdiffusive electrons excited in the Al enter the Ni layer. Upon entering the Ni layer, the two spin channels experience very different transport properties. Spin-majority electrons are unimpeded as they traverse the Ni layer, eventually reaching the Fe layer. Conversely, spin-minority electrons accumulate within the first half nm in the Ni layer. Second, electrons that are directly excited in the Ni layer exhibit a different behavior. Non-equilibrium spin-majority electrons in Ni can easily superdiffuse out of the layer, transferring spin angular momentum into the neighboring layers, thereby causing an induced magnetization change in Fe and Al (Supplementary Figure S1). Spin-minority electrons excited in the Ni layer are immobilized by scattering in the region where they

are created, to a first approximation. Third, electrons are also excited in the Fe layer, with the amount of excited electrons depending on the laser fluence reaching the Fe. However, the excited hot electrons in Fe do not exhibit the same good transport properties as those of Ni or Al; the spin transport asymmetry for Fe is weaker, and both spin channels are less amenable to superdiffusion. Hence, with the aim of having an intuitive understanding of the superdiffusion in this layered structure, we can approximately assume that spin-majority and -minority excited electrons are essentially trapped once they enter the Fe. This further explains the small difference in ΔM for Fe shown in Supplementary Figures S1a and S1b.

One must also consider that the electron transport does not evolve in a purely ballistic way but rather the electrons undergo inelastic electron-electron scatterings in the layers. In addition, they can be reflected at the surfaces and interfaces. Screened electrons escaping from the Ni layer become mainly trapped in the Fe layer. Even screened electrons that superdiffuse first into the Al layer can be reflected at the Al-vacuum interface and travel back towards the Fe layer, because of the good transport properties of Al. We emphasize that the calculated results shown in Supplementary Figure S1 have been obtained by solving the superdiffusive equation with the proper transport quantities – the purpose of the simplified explanation above only serves to assist in an intuitive analysis of the data.

Fluence-dependent time- and layer-resolved magnetization measurements, further confirming the above model, are discussed in some detail in Supplementary Figure S2.

SUPPLEMENTARY METHODS

In our experiment, the magnetic signal is measured in the transverse magneto-optical Kerr effect (T-MOKE) geometry (Supplementary Figure S3). The reflected amplitude of linear *p*-polarized light depends on the magnetization component of the sample oriented perpendicular to the plane of incidence. Defining the magnetic asymmetry A by Eq.(1) of the main text, it is possible to relate A to the dielectric properties of the sample. Assuming ε_{xx} to be the diagonal element of the dielectric tensor, ε_{xy} the off-diagonal element, ε_0 the vacuum dielectric permittivity and Φ the angle of incidence, the expression for A for a single-element film becomes[36]

$$A = \mathrm{Re}\left(\frac{2\varepsilon_0 \varepsilon_{xy} \sin(2\Phi)}{\varepsilon_{xx}^2 \cos^2(\Phi) - \varepsilon_0 \varepsilon_{xx} + \varepsilon_0^2 \sin^2(\Phi)} \right). \qquad \text{(S1)}$$

At the atomic absorption edges, the off-diagonal element of the dielectric tensor ε_{xy} is resonantly enhanced and therefore, the magnetic asymmetry is increased from less than one percent in the visible spectral range[37], up to tens of percent[23]. The increase of ε_{xy} over its analogue in the visible spectral range is due to the large spin-orbit and exchange splitting of the *3p* shallow core states[38]. The magnetic asymmetry signal becomes additionally amplified at the pseudo-Brewster angle[23]. In our experiment, we generate a spectrum of high harmonics with photon energies spanning the XUV region. (Harmonics up to the absorption edge of Al (72.6 eV [http://henke.lbl.gov/]) are used to probe the sample). This enables us to perform spectroscopic measurements at the Fe and Ni *3p* absorption edges (52.7 eV and 66 eV, respectively), probing the magnetic response of both elements simultaneously. The experimental asymmetry data can be reproduced by simulations based on the Maxwell equations with appropriate boundary conditions[39,40]. The time-resolved magnetic asymmetry was fit to a double exponential function

$$A(t) = 1 - \Delta A\left[1 - \exp\left(-(t - t_0)/\tau_m\right)\right]\exp\left(-(t - t_0)/\tau_r\right), \qquad \text{(S2)}$$

adopted from [41], where ΔA denotes the quenching amplitude of the magnetization, t_0 the offset from the time zero, and τ_m and τ_r are the de- and remagnetization times. We analyzed the time-resolved magnetic asymmetry data by integrating over the *3p* absorption edge of Ni and Fe and normalizing the magnetic asymmetry to values obtained prior to laser excitation. The demagnetization (τ_m) and remagnetization (τ_r) times extracted from time-resolved T-MOKE measurements and fit using Supplementary Eq. S2 are shown in Supplementary Table S1.

SUPPLEMENTARY REFERENCES

36. Oppeneer, P. M. Magneto-optical Kerr spectra in Buschow, K. H. J. (ed.) Handbook of magnetic materials **13**, Elsevier, 229–422 (2001).

37. Afonso, C., Lagunas, A., Briones, F. & Girón, S. Magneto-optic Kerr effect in amorphous Fe_xSi_{1-x}. *Journal of Magnetism and Magnetic Materials* **15**, 833–834 (1980).

38. Valencia, S., Kleibert, A., Gaupp, A., Rusz, J., Legut, D., Bansmann, J., Gudat, W. & Oppeneer, P.M. Quadratic x-ray magneto-optical effect upon reflection in near-normal incidence configuration at the M edges of 3d transition metals. *Phys. Rev. Lett.* **104**, 187401 (2010).

39. Yeh, P. Optics of anisotropic layered media: a new 4 x 4 matrix algebra. *Surface Science* **96**, 41–53 (1980).

40. Visnovsky, S. Optics of magnetic multilayers. *Czechoslovak Journal of Physics* **41**, 663-693 (1991).

41. Guidoni, L., Beaurepaire, E. & Bigot, J.-Y. Magneto-optics in the ultrafast regime: thermalization of spin populations in ferromagnetic films. *Phys. Rev. Lett.* **89**, 017401 (2002).